JOURNAL OF SOLID STATE CHEMISTRY **132,** 139–143 (1997)
ARTICLE NO. SC977432

Magnetic and Electrical Properties of $Bi_{1-x}Sr_xMnO_3$: Hole-Doping Effect on Ferromagnetic Perovskite $BiMnO_3$

H. Chiba, T. Atou, and Y. Syono

Institute for Materials Research, Tohoku University, Katahira, Aoba-ku, Sendai 980-77, Japan

Received December 18, 1996; in revised form April 14, 1997; accepted April 15, 1997

Although La^{3+} and Bi^{3+} ions have similar ionic radii, the $Bi_{1-x}Sr_xMnO_3$ system was found to show quite different behavior from $La_{1-x}Sr_xMnO_3$ in which ferromagnetism with metallic conductivity is achieved by the "double exchange mechanism." $BiMnO_3$ which was synthesized under high pressure is a ferromagnetic insulator with $T_c = 105$ K, in contrast to antiferromagnetic $LaMnO_3$. Though Sr substitution in $BiMnO_3$ increased conductivity, no metallic state was achieved up to the solid solution limit of $x = 0.67$. Furthermore the saturation magnetic moment of 3.6 μ_B observed in $BiMnO_3$ decreased very rapidly with increasing x, and ferromagnetism disappeared for $x > 0.4$. These observations suggest that the highly polarizable Bi^{3+} ion with $6s^2$ lone pair would cause local distortion of the perovskite lattice, which presumably reduces the mobility of carriers. The origin of ferromagnetism in $BiMnO_3$ requires a mechanism other than the double exchange theory. © 1997 Academic Press

1. INTRODUCTION

Recently the ferromagnetism of perovskite solid solutions $(La, AE)MnO_3$ (AE = Ca, Sr, Ba) (1, 2) has attracted renewed interest due to colossal magnetoresistance (CMR) (3–8) and magnetic field-induced structural phase transition (9). In $LaMnO_3$, which exhibits antiferromagnetism (10), the Mn^{3+} ion has three electrons in the lower threefold degenerate t_{2g} orbitals and one excess electron in the upper twofold degenerate e_g orbital. Replacement of La^{3+} with AE results in carrier creation due to hole-doping. This mobile carrier causes ferromagnetism via coupling with localized t_{2g} spins, which is well known as the so-called double exchange mechanism (11–13).

On the other hand, $BiMnO_3$, which can be synthesized under high pressure (14, 15), shows a large ferromagnetic moment without hole-doping. Compared with antiferromagnetic $LaMnO_3$, this ferromagnetism should be noted because both Bi^{3+} (1.24 Å) and La^{3+} (1.22 Å) have very similar ionic radius (16). (The number in parentheses is the value for 9-coordination.) The difference in the electronic configuration would be a key to understanding the origin of ferromagnetism. For example, $BiMnO_3$ (triclinic) is remarkably more distorted than $LaMnO_3$ (monoclinic), which could be explained by a highly polarizable $6s^2$ character of Bi^{3+} (14). The main purpose in this work is to clarify the origin of the ferromagnetism in $BiMnO_3$. In order to see a possibility of the double exchange mechanism in this compound, hole-doping by Sr^{2+} substitution was examined. A distinct feature due to $6s^2$ character of Bi^{3+} in $Bi_{1-x}Sr_xMnO_3$ will be shown and its magnetic and electrical properties will be discussed in comparison with $La_{1-x}Sr_xMnO_3$.

2. EXPERIMENTAL

The synthesis of polycrystalline samples of $Bi_{1-x}Sr_xMnO_3$ with $x = 0$, 0.1, 0.2, 0.3, 1/3, 0.5, 2/3, 0.8, and 0.9 was carried out by using a conventional ceramic technique and a high-pressure technique. Starting materials and synthesis conditions are summarized in Table 1. Specimens with the composition of $0.3 \leq x \leq 2/3$ were obtained at ambient pressure by using a conventional ceramic technique. The firing conditions were carefully selected as described in Table 1 for better crystallization. We repeated firing followed by grinding several times. A slight Bi deficiency, which was examined by inductively coupled plasma (ICP) analysis, was introduced in the course of firing. In order to prepare more stoichiometric specimens we added extra Bi_2O_3 before the final firing. Specimens with the composition of $1 > x \geq 0.8$ could not be obtained as a single phase because of the stable hexagonal $SrMnO_3$ (18).

For the composition of $x \leq 0.2$, high pressure synthesis was required.[1] The raw material was stirred with acetone for 15 min in a ball mill and was dried. Then the residual mixture was sealed in a gold capsule (ϕ 3 × 5 mm) to isolate

[1] We failed to prepare single crystal of $BiMnO_3$ with starting material of $2Bi_2O_3 + Mn_2O_3$ at ambient pressure according to Bokov *et al.* (see Ref. 21). This attempt resulted in Bi_2O_3 and $Bi_2O_3 \cdot 2Mn_2O_3$ with a trace amount of $BiMnO_3$.

0022-4596/97 $25.00

TABLE 1
Starting Materials and Synthesis Conditions

Nominal composition (x)	Starting materials[a]	Synthesis condition		
		Prefiring	Final firing[b]	Pressure
0	$Bi_2O_3 + Mn_2O_3$	—	600°C for 3 h	4 GPa
0.1	$9/2Bi_2O_3 + 9/2Mn_2O_3 + SrMnO_3$	—	800°C for 1 h	4 GPa
0.2	$(1-x)/2Bi_2O_3 + 1/2Mn_2O_3 + xSrCO_3$	780°C in N_2[c]	700°C for 2 h	4 GPa
0.3, 1/3	$(1-x)/2Bi_2O_3 + 1/2Mn_2O_3 + xSrCO_3$	750°C in air	900°C in N_2	1 atm
0.5, 2/3	$(1-x)/2Bi_2O_3 + 1/2Mn_2O_3 + xSrCO_3$	900°C in air	1200°C in air	1 atm

[a] Mn_2O_3 was calcined in air at 700°C for several days for proper valence and weighing.
[b] Firing temperature was gradually raised from prefiring temperature up to this temperature.
[c] Starting materials were prefired before pressing.

from reductive surroundings and placed in a cylindrical graphite which served as a heater. This is different from that described in the previous work (14, 15) in which the starting materials with excess Bi_2O_3 was directly packed in a graphite capsule. The sample assembly was set in a cube ($12.5 \times 12.5 \times 12.5$ mm^3) made of pyrophyllite and subjected to high pressure using a DIA-10 type cubic press. In the case of $BiMnO_3$ ($x = 0$), the starting materials were heated at 4 GPa and 600°C according to the previous work (14, 15). It took 3 h to diminish impurities. We had more impurities when the specimen was heated at higher temperature. In the case of $x = 0.1$ and 0.2, at first we examined following procedures; mixture of $(1-x)/2Bi_2O_3 + 1/2Mn_2O_3 + xSrCO_3$ was prefired in 1 atm nitrogen atmosphere and submitted to pressing and heating. $Bi_{0.8}Sr_{0.2}MnO_3$ ($x = 0.2$) was successfully synthesized maintaining the temperature of 700°C at 4 GPa for two hours by this method. However $Bi_{0.9}Sr_{0.1}MnO_3$ ($x = 0.1$) required another process. $Bi_{0.9}Sr_{0.1}MnO_3$ was obtained by changing the starting materials in which $SrMnO_3$ was added to the mixture of 9/2 Bi_2O_3 + 9/2 Mn_2O_3 to adjust the oxygen stoichiometry. This synthesis required a temperature of 800°C at 4 GPa for 1 h.

The prepared specimens were examined by X-ray powder diffraction (XRD) using a monochromated Cu$K\alpha$ radiation. XRD indicated that specimens synthesized at ambient conditions were single phase, whereas specimens synthesized under high pressure contained a small amount of unidentified impurites. The unit cell dimensions were determined from the observed d-spacings by least squares method. The analyses of the chemical composition of the final products synthesized at ambient pressure were carried out using the ICP analysis and the iodine titration method, which showed the nearly identical metallic and oxygen stoichiometry with the nominal composition, respectively.

Magnetization (M) was measured in a magnetic field up to 5 T in the temperature range of 5–350 K with a superconducting quantum interference device magnetometer (Quantum Design). The Curie temperature (T_c) was determined with a magnetic field of 100 Oe. DC resistivity measurements were performed using conventional four-probe, or quasi-four-probe, method with a measuring current of 0.1 mA. Electrodes were formed by pressing indium onto the sample.

3. RESULTS AND DISCUSSION

3.1. Structural Aspects

Typical XRD patterns of the prepared specimens with $x = 0.1$, 0.3, and 0.5 are shown in Fig. 1. The reflection peaks were indexed on the basis of the perovskite lattice with $a = c \approx b \approx a_p$, where a_p is a lattice parameter of the

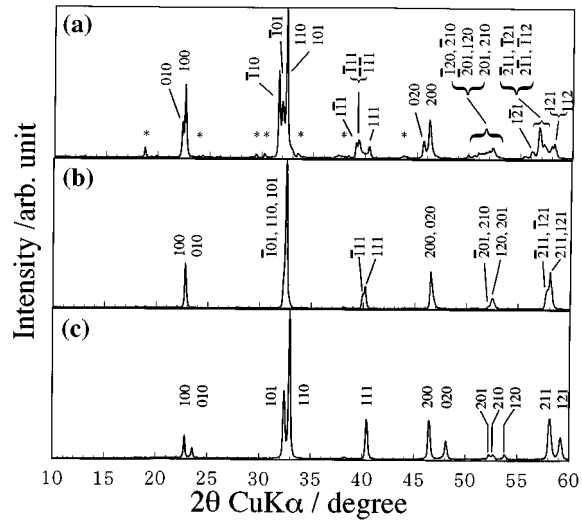

FIG. 1. Typical XRD patterns at room temperature (a) for triclinic $Bi_{0.9}Sr_{0.1}MnO_3$, (b) for monoclinic $Bi_{0.7}Sr_{0.3}MnO_3$, and (c) for tetragonal $Bi_{0.5}Sr_{0.5}MnO_3$. The asterisk indicates peaks of impurity compounds. Although the XRD pattern of $Bi_{0.7}Sr_{0.3}MnO_3$ is close to pseudo-cubic, a monoclinic unit-cell is adopted because a slight splitting of the (1 1 1) peak is observed.

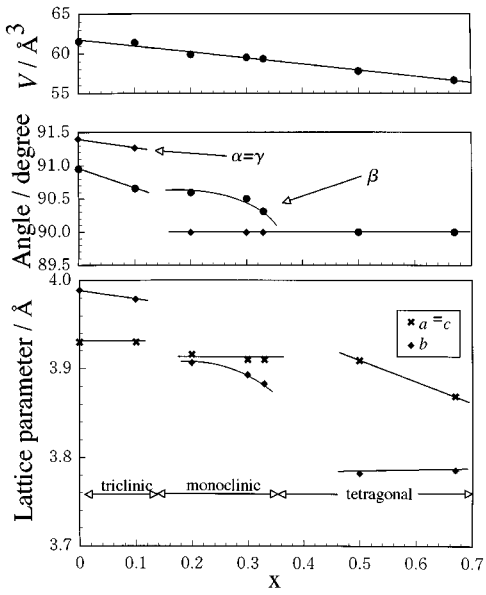

FIG. 2. The compositional change of lattice parameters at room temperature in the system $Bi_{1-x}Sr_xMnO_3$.

cubic perovskite. The structural transformation of $Bi_{1-x}Sr_xMnO_3$ with increasing x was represented by triclinic $\Rightarrow$ monoclinic $\Rightarrow$ tetragonal lattices on this basis, although the actual symmetry is higher than them, i.e., monoclinic ($a \approx c \approx \sqrt{2}a_p$, $b \approx a_p$) $\Rightarrow$ orthorhombic ($a \approx c \approx \sqrt{2}a_p$, $b \approx a_p$) $\Rightarrow$ tetragonal ($a = c \approx b \approx a_p$), respectively. The tetragonal distortion was observed at room temperature neither in $Bi_{1-x}Ca_xMnO_3$ (19, 20) nor in $La_{1-x}Sr_xMnO_3$ which reveals an orthorhombic to rombohedral change (9). Extra peaks of XRD of our oxides could not be assigned to superlattice reflections, though Bokov *et al.* (21) and Zuotao *et al.* (22) reported $a = c \approx b \approx 2a_p$ for the triclinic $BiMnO_3$ and $a = b \approx 2a_p$, $c \approx a_p$ for the tetragonal $Bi_{0.5}Sr_{0.5}MnO_3$, respectively. The change of the lattice parameters is shown as a function of x in Fig. 2. The changes in the a- and c-axis with x are very little, but the b-axis becomes contracted with increasing x. In spite of discontinuous changes of lattice parameters with different symmetry, the cell volume linearly decreases with increasing x, which corresponds to the systematic increase of the Mn^{4+} content by Sr^{2+} substitution for Bi^{3+}. The difference among cell parameters seems to become smaller with the increase in x; therefore the unit cell is expected to tend to be more isotropic in the Sr^{2+}-rich composition. This phenomenon is associated with reduction of the Jahn–Teller effect and/or that of the lone-pair character of Bi^{3+}. Shannon (16) has shown a criterion of how the lone-pair character of Bi^{3+} affects the cell volume of Bi^{3+} compounds with respect to the isotypic compounds of La^{3+}; that is, when the lone-pair character is dominant, the Bi^{3+} compound is distorted, and Bi^{3+} and La^{3+} compounds have approximately equal volumes with the cell–volume ratio of 1.00–1.03. On the other hand, in the case that the lone-pair character of Bi^{3+} is largely suppressed, the compounds take higher symmetry and the cell–volume ratio is reduced to 0.90–0.98. In the present case, $Bi_{1-x}Sr_xMnO_3$ is more distorted than $La_{1-x}Sr_xMnO_3$, and the ratio of formula volume was found to be 0.99–1.02. Therefore the lone-pair character of Bi^{3+} is evidently dominant in $Bi_{1-x}Sr_xMnO_3$.

3.2. Magnetic and Electrical Properties

The temperature dependence of magnetization and inverse of molar magnetic susceptibility (χ_m) of $BiMnO_3$ are shown in Fig. 3a. $BiMnO_3$ showed a ferromagnetic transition at 105 K, and a magnetic moment of 2.6 μ_B at 77 K measured in a field of 1 T, consistent with the previous work (14, 15, 21). The relationship of $1/\chi_m$ vs T obeys the Curie–Weiss law above T_c, yielding 120 K for the paramagnetic Curie temperature (Θ_p) and 5.10 μ_B for the effective magnetic moment (p_{eff}). The former is slightly higher than T_c, and the latter is slightly larger than the calculated value of 4.90 μ_B by assuming the spin-only J value. The magnetization curve of $BiMnO_3$ at 5 K is shown in Fig. 4a. A small gradual increase of the magnetization was found even above 2 T and the measured magnetic moment at 5 T was 3.6 μ_B which was slightly smaller than that of the fully aligned value of 4 μ_B. This is in contrast to the ferromagnetic behavior in $La_{1-x}Sr_xMnO_3$, in which magnetization was easily saturated at 0.4 T.

When Bi^{3+} was partially replaced with Sr^{2+}, the magnetization below T_c rapidly decreased and T_c became ambiguous (Figs. 3b, and 5). For the composition of $x \geq 0.5$, a clear magnetic transition was no longer observed.

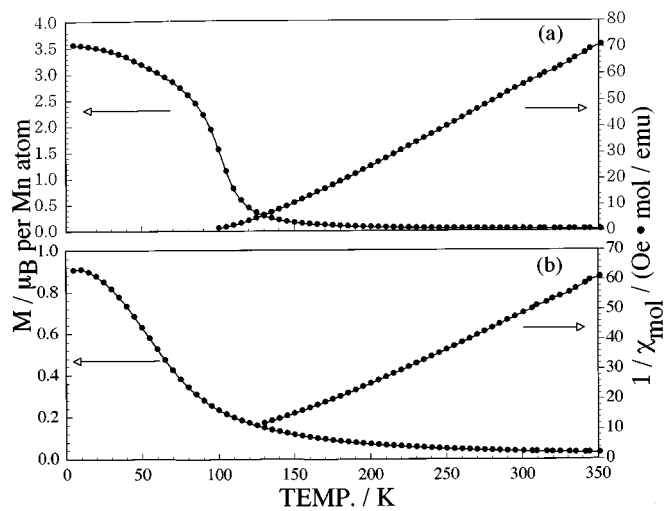

FIG. 3. Temperature variation of magnetization and inverse of molar magnetic susceptibility of $BiMnO_3$ (a) and of $Bi_{0.7}Sr_{0.3}MnO_3$ (b) measured at 1T.

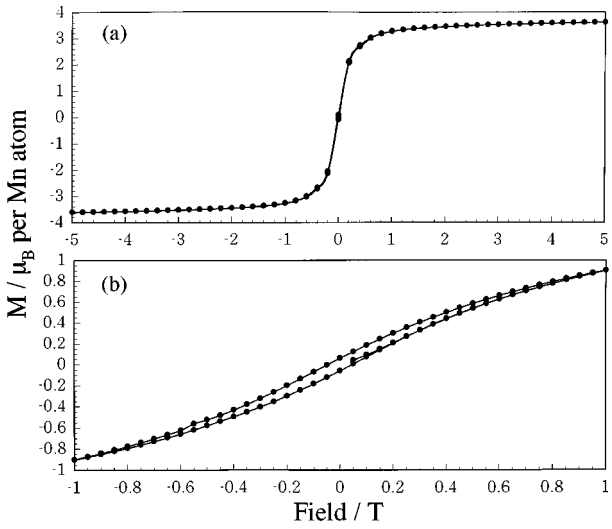

FIG. 4. Magnetization cuve of $BiMnO_3$ (a) and of $Bi_{0.7}Sr_{0.3}MnO_3$ (b) measured at 5 K.

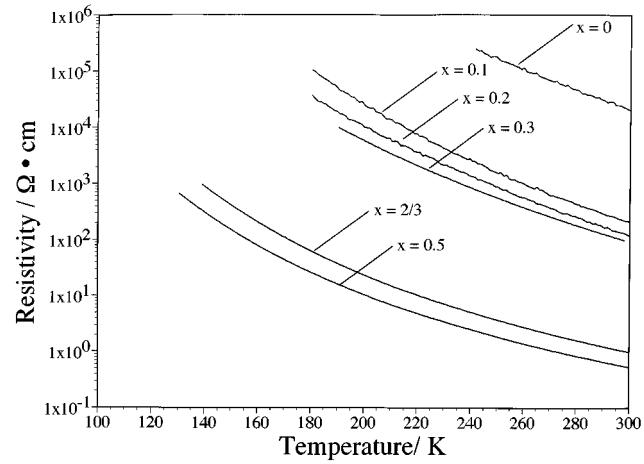

FIG. 6. Electrical resistivity vs temperature in the system $Bi_{1-x}Sr_xMnO_3$.

Furthermore hysteresis was observed even in a field higher than 1 T for the composition of $x \geq 0.2$ (Fig. 4b). The composition dependence of T_c and Θ_p are shown in Fig. 5. The T_c is almost constant with a very slight decrease with the increase in x, in contrast to $La_{1-x}Sr_xMnO_3$ in which T_c increases with the increase in x and reaches the maximum around $x = 0.4$. The Θ_p is slightly higher than T_c due to downward curvature of $1/\chi_m$ vs T plots and tends to decrease with the increase in x, indicating that the ferromagnetic exchange becomes weaker.

The electrical resistivity (ρ) measurements were carried out down to 20 K, but resistivities of all the specimens showed a semiconducting temperature dependence and became too high to measure at low temperatures. The temperature dependence of electrical resistivity is shown in Fig. 6. The magnitude of the resistivity decreased with the increase in x due to hole doping and reaches a minimum at $x = 0.5$ (for example see the data at 298 K in Table 2), but all specimens show a thermally activated behavior of a typical semiconductor. The calculated activation energy (E_a) decreases with the increase in x, consistent with the decrease in resistivity (Table 2). The insulator to metal transition as was observed in $La_{1-x}Sr_xMnO_3$ was not observed in $Bi_{1-x}Sr_xMnO_3$.

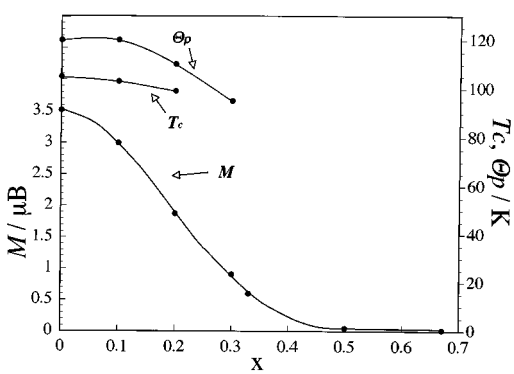

FIG. 5. The composition dependence of magnetization per a Mn atom measured at 5 K with a magnetic field of 1 T, Curie temperature (T_c) and paramagnetic Curie temperature (Θ_p) of $Bi_{1-x}Sr_xMnO_3$. T_c and Θ_p of other compositions could not be determined because of ambiguity.

3.3. *Comparison with $La_{1-x}Sr_xMnO_3$*

In $La_{1-x}Sr_xMnO_3$ (6–8), the ferromagnetic state appears for the composition $x \geq 0.1$. Electrical resistivity decreases with the increase in x, accompanying a paramagnetic insulator to ferromagnetic metal transition for $0.175 \leq x \leq 0.3$ and a paramagnetic metal to ferromagnetic metal transition for $x \geq 0.3$. This itinerancy-correlated picture follows the double exchange scenario. On the contrary, in $Bi_{1-x}Sr_xMnO_3$ the magnetic moment rapidly decreases with the increase in x and the electrical resistivity remains thermally activated; hence the transition to a metallic state does not occur, indicating that the double exchange mechanism does not work in this system. This is probably caused by some localization effect derived from the local distortion due to the aforementioned lone-pair character. In conclusion, the interpretation of ferromagnetism of $BiMnO_3$ requires a mechanism other than the double exchange theory. The importance of the orbital ordering of Mn ions in the perovskite lattice has been pointed out (17). For example, ferromagnetic arrangement within c layer in the antiferromagnetic $LaMnO_3$ was explained by a ferromagnetic exchange interaction due to the e_g orbital of Mn^{3+} ions perpendicular to each other. To clarify the origin of the ferromagnetism in $BiMnO_3$, an accurate structural analysis is indispensable.

TABLE 2
Summary of Magnetic and Electrical Properties of $Bi_{1-x}Sr_xMnO_3$

Nominal composition (x)	M at 5 K with a field of 1 T (μ_B per Mn atom)[a]	T_c (K)	Θ_p (K)	p_{eff} (μ_B per atom)[b]	ρ at 298 K ($\Omega \cdot$cm)	E_a (eV)[c]
0	3.51 (4.0)	105	120	5.10 (4.90)	2.31×10^4	0.262
0.1	2.99 (3.9)	103	120	5.01 (4.80)	2.23×10^2	0.243
0.2	1.87 (3.8)	99	110	5.30 (4.69)	1.34×10^2	0.222
0.3	0.90 (3.7)	—[d]	95	5.67 (459)	9.92×10	0.211
1/3	0.59 (3.67)	—[d]	—[d]	—[d]	—[e]	
0.5	0.04 (3.5)	—[f]	—[f]	—[f]	5.56×10^{-1}	0.143
2/3	0.01 (3.33)	—[f]	—[f]	—[f]	1.04	0.155

[a]The number in parentheses show calculated value by assuming the ferromagnetic arrangement.
[b]Effective magnetic moment calculated from measured susceptibility for the temperature range up to 350 K. The number in parentheses show calculated value by assuming spin only J value.
[c]Activation energy calculated on the basis of $\rho = \rho_0 \exp(E_a/kT)$.
[d]Not determined because of ambiguity.
[e]Measurement was not carried out.
[f]There is no clear magnetic transition.

ACKNOWLEDGMENT

We thank T. Nishizaki (IMR, Tohoku Univ.) for his help in the magnetic measurement with a field of 5 T. We thank M. Kikuchi and K. Kusaba (IMR, Tohoku Univ.) for useful discussions and assistance and also H. Faqir (Laboratoire de Physico-Chimie des Matériaux, Equipe de Chimie du Solide, Université de Provence), who tried the synthesis of $BiMnO_3$ at ambient pressure. The ICP analysis was performed at Laboratory for Developmental Research of Advanced Materials, IMR. This work was partly supported by a Grant-in-Aid for Scientific Research on Priority Areas, "Anomalous Metallic State near the Mott Transition," of the Ministry of Education, Science and Culture, Japan.

REFERENCES

1. G. H. Jonker and J. H. Van Santen, *Physica* **16,** 337 (1950).
2. G. H. Jonker, *Physica* **22,** 707 (1956).
3. R. von Helmolt, J. Wecker, B. Holzapfel, L. Schultz, and K. Samwer, *Phys. Rev. Lett.* **71,** 2331 (1993).
4. S. Jin, T. H. Tiefel, M. McCormack, R. A. Fastnachit, R. Ramesh, and L. H. Chen, *Science* **264,** 413 (1994).
5. P. Schiffer, A. P. Ramirez, W. Bao, and S.-W. Cheong, *Phys. Rev. Lett.* **75,** 336 (1995).
6. Y. Tokura, A. Urushibara, Y. Moritomo, T. Arima, A. Asamitsu, G. Kido, and N. Furukawa, *J. Phys. Soc. Jpn.* **63,** 3931 (1994).
7. T. Tokura, A. Urushibara, Y. Moritomo, A. Asamitsu, Y. Tomioka, T. Arima, and G. Kido, *Mater. Sci. Eng. B* **31,** 187 (1995).
8. A. Urushibara, Y. Moritomo, T. Arima, A. Asamitsu, G. Kido, and Y. Tokura, *Phys. Rev. B* **51,** 14103 (1995).
9. A. Asamitsu, Y. Moritomo, Y. Tomioka, T. Arima, and Y. Tokura, *Nature* **373,** 407 (1995).
10. E. O. Wollan and W. C. Koehler, *Phys. Rev.* **100,** 545 (1955).
11. P. W. Anderson and H. Hasegawa, *Phys. Rev.* **100,** 675 (1955).
12. P.-G. de Gennes, *Phys. Rev.* **118,** 141 (1960).
13. K. Kubo and N. Ohata, *J. Phys. Soc. Jpn.* **33,** 21 (1972).
14. F. Sugawara, S. Iida, Y. Syono, and S. Akimoto, *J. Phys. Soc. Jpn.* **25,** 1553 (1968).
15. F. Sugawara, S. Iida, Y. Syono, and S. Akimoto, *J. Phys. Soc. Jpn.* **20,** 1529 (1965).
16. R. D. Shannon, *Acta Crystallogr. A* **32,** 751 (1976) and references therein.
17. J. B. Goodenough, *Phys. Rev.* **100,** 564 (1955).
18. T. Negas and R. S. Roth, *J. Solid State Chem.* **1,** 409 (1970).
19. V. A. Bokov, N. A. Grigoryan, and M. F. Bryzhina, *Physica Status Solidi* **20,** 745 (1967).
20. H. Chiba, M. Kikuchi, K. Kusaba, Y. Muraoka, and Y. Syono, *Solid State Commun.* **99,** 499 (1996).
21. V. A. Bokov, I. E. Myl'nikova, S. A. Kizhaev, M. F. Bryzhina, and N. A. Grigoryan, *Sov. Phys. Solid State* **7,** 2993 (1966).
22. Z. Zuotao, R. Yufang, and M. Jian, *Mater Res Bull.* **28,** 1329 (1993).